Mixed Effects of the Atomic Arrangement and Surface Chemistry on the Electrodeposition of Bi Thin Films on n-GaAs Substrates

Alicia Prados[1], *Lucas Pérez*[1], *Álvaro Guzmán*[2], *Rocío Ranchal*[1]*

1. Dept. Física de Materiales, Universidad Complutense de Madrid, 28040, Madrid, Spain,
2. Instituto de Sistemas Optoelectrónicos y Microtecnología. Universidad Politécnica de Madrid, 28040, Madrid, Spain

ABSTRACT

We have studied the electrodeposition of Bi thin films on two GaAs orientations with different atomic arrangement and chemical composition, (110) and (111)B. The electrochemical properties of each substrate have been analyzed by means of cyclic voltammetries and current transients. Then, x-ray diffraction has been used to determine the crystal structure and quality of the Bi films, and atomic force microscopy images have provided information about the surface morphology. Finally, the Bi/GaAs interface has been electrically characterized by means of capacitance-voltage and current-voltage curves. In this study, we have been able to discriminate between the effect of surface chemistry and the arrangement of surface atoms. The former has a direct effect on the reduction process of Bi(III) ions and on the electrical properties of the Bi/GaAs interface, whereas the atoms arrangement at the substrate surface determines the texture and morphology of the Bi films.

Introduction

Bismuth (Bi) has received in-depth attention in the last years due to its interesting electronic properties [1-4]. On one hand, the strong spin-orbit coupling present in this material is responsible for its peculiar band structure, characterized by a highly anisotropic Fermi surface [5-7]. As a result, carriers mass reaches extremely low values in certain crystal directions, $m^* = (1\text{-}6)\cdot 10^{-3}\ m_e$ [6-8], which in turn leads to high mobilities. In addition, the Bi rhombohedral structure (R-3m) induces a semimetallic behaviour that results in a low carrier density, $n = 2.75 \cdot 10^{17}\ cm^{-3}$ [7-9]. These two characteristics makes Bi a suitable scenario for the study of classical and quantum size effects (SE and QSE) on the electronic properties, since carriers mean free path [10-11] and Fermi wavelength [5, 12] are larger than those obtained in other materials. In addition, Bi surface states are strongly spin-polarized via Rashba effect [13], which could make Bi to have a strong impact in spintronics [14]. Very recently, a large spin to charge conversion induced by spin-orbit coupling in a Bi/Ag Rashba interface has been measured [15]. The study of these effects and their dependence on crystal direction can be carried out on different nanostructured systems. Although there are some works on nanowires [16-17], thin films represent a better starting point as only one dimension is reduced. In addition, thin films are more compatible with standard processing techniques, which would eventually allow the integration of Bi films in devices.

To prevent current leakage during transport measurements in Bi thin films, low-doped semiconducting substrates should be used because they guarantee the existence of a wide Schottky barrier between the Bi layer and the substrate. However, highly-doped semiconductors are also interesting to study since thermionic field emission through Schottky barriers is promising for spin injection/detection [18]. For these purposes, electrodeposition has proved to be a suitable technique since high-quality Bi thin films, and other metallic layers, can be grown onto

semiconducting substrates. In fact, high-quality Bi films have been electrodeposited on n-GaAs single-crystal substrates, leading to Bi/GaAs Schottky diodes [19-22]. The use of single-crystal semiconductors as substrates makes necessary the knowledge of its crystal structure and chemical composition because both of them lead to the specific energy band structure and, therefore, the specific electronic properties of the semiconductor. However, the breaking of the 3D translation symmetry at the substrate surface supposes the appearance of dangling bonds that act as states in the middle of the gap. The density, geometry and charging character of the dangling bonds (donor or acceptor states depending on the atom) depends on the substrate orientation, leading to different surface state band structures [23-25]. Therefore, the surface orientation strongly affects the electrochemical properties of the substrate surface and the electrical properties of the metal-semiconductor interface [24, 26-28]. Although other authors have studied the electrodeposition of Bi on GaAs substrates with different surface orientations [19, 29-31], the discrimination between the effect of surface atomic arrangement and surface chemistry has not been done yet.

In this work, we have investigated the influence of substrate orientation on the electrodeposition of Bi thin films on n-GaAs substrates. Two orientations with different atomic arrangement and chemical composition have been compared: (110) and (111)B. Our results show that surface composition has a direct effect on the reduction process of Bi(III) ions and on the electrical properties of the Bi/GaAs interface, whereas surface atoms arrangement determines the texture and morphology of the Bi films.

Experimental Methods

Electrochemical experiments have been carried out using a stable water-based electrolyte containing 1 mM Bi_2O_3 (bismuth oxide) as Bi(III) cations source and 1 M $HClO_4$ (perchloric

acid) as supporting electrolyte. Solutions were prepared with analytical grade chemicals and deionized water in order to avoid free ions. Bismuth oxide was firstly added to perchloric acid in a volumetric flask and then, the solution was made to the mark with deionized water. The pH of the solution (approximately 0.1) was not necessary to be further adjusted.

Working electrodes were Si doped n-type GaAs(110) and GaAs(111)B wafers, supplied by Geo Semiconductors, with a carrier concentration of $(0.9 – 1) \times 10^{18}$ cm^{-3} and $(0.85 – 0.95) \times 10^{18}$ cm^{-3}, respectively. A similar carrier concentration in both orientations is mandatory since this parameter affects the electrochemical properties of semiconducting substrates. Ohmic contacts were made on the back of the wafers by thermal evaporation of 80 nm of AuGe (2% Ge) and 250 nm of Au, followed by an annealing at 380 ^{o}C in forming gas for 90 s. The total surface area exposed to the electrolyte was 0.15 cm^2 in all cases. Prior to each experiment, substrates were degreased and then etched to remove GaAs native oxide under darkness conditions. Firstly, substrates are dipped in a solution of HCl (10% vol.) for 2 minutes to remove arsenic and gallium oxides [32]. Then, substrates are rinsed in deionized water for 2 minutes to remove Ga-Cl_x species since they are soluble in water [33]. Finally, substrates are immersed in 1 M $HClO_4$ (supporting electrolyte) for 2 minutes to remove possible Cl^- ions remaining in the solution or adsorbed at the substrate surface. Then, the substrate surface is protected from air with a drop of 1M $HClO_4$ (supporting electrolyte) when transferred to the Bi(III) solution, where substrates remained 2 minutes to reach a stable Open Circuit Potential (OCP). In this condition, the substrate surface is oxide-free with about one monolayer coverage of elementary As, which interacts with the protons in the solution (As-H) [34-35].

The electrochemical properties of each orientation have been studied by means of cyclic voltammetries (CV) and current transients. These experiments were performed in a three-

electrode cell with a platinum mesh as counter electrode and a Ag/AgCl (3 M NaCl) reference electrode supplied by BASi (E_{eq} = 0.196 V vs. SHE). In this study, all potentials are referred to this electrode. Electrochemical experiments were controlled by a Metrohm Autolab PGSTAT302N potentiostat. After deposition, films were rinsed in deionized water and dried with N_2. The nominal thickness of the films was controlled by Faraday's law:

$$Q(mC) = \frac{\rho \cdot z \cdot F}{M \cdot \kappa} \cdot S \cdot d = 3.48 \cdot S(cm^2) \cdot d(nm) \quad (1)$$

where ρ is Bi density (9.8 g $\cdot cm^{-3}$), z is the number of electrons involved in the reduction reaction of Bi(III) ions (3), *F* is Faraday's constant (96485 C$\cdot$mol^{-1}), *M* is Bi molecular weight (208.98 g$\cdot$ mol^{-1}), κ is the process efficiency, *S* is the area of the working electrode in cm^2 and *d* is the film thickness in nm. In order to obtain a Bi thickness of 40 nm, it is necessary to consider a κ of nearly 40 %. Thus, a charge of 20.88 mC was transferred in each growth.

The influence of the substrate surface orientation on the crystal structure and morphology of the Bi films has been determined by X Ray Diffraction (XRD) and Atomic Force Microscopy (AFM). Structural characterization was done by XRD using a Philips X'Pert PRO system equipped with a Cu target ($\lambda_{K\alpha}$ = 1.54 nm) and a four-circle goniometer. All films were measured in both asymmetric and symmetric configurations. Grazing incidence mode (GIXRD), also called grazing incidence asymmetric-Bragg diffraction (GIABD), was used to analyze the crystal structure of the Bi films. The incidence angle (ω) was set in the range of $0.5^o - 1^o$. Then, Bragg-Brentano configuration ($\theta - 2\theta$ scan) was used to determine the preferred orientation of the films. To avoid substrate reflections, an offset of 0.5^o was introduced between the incidence and the diffracted direction ($\omega = \theta - \theta_{offset}$). In order to study the out-of-plane and in-plane crystal quality, ω-rocking curves and φ-scans have been performed, respectively. The average tilt

and twist of Bi grains with respect the GaAs substrate is defined as one half of full width at half maximum (FWHM/2) of ω-rocking curves and φ-scans, respectively. Surface characterization was done by means of a Nanoscope AFM with a Si tip, working in tapping mode and operating in air. Images were analyzed with WSxM 5.0 software and Nanoscope 5.31r1 software.

Finally, the Bi/GaAs interface was characterized electrically by means of capacitance - voltage (C-V) and current-voltage (I-V) curves. Several diodes with 200 μm of diameter were fabricated in the Bi films by standard optical lithography followed by photochemical etching. Afterwards, an electrical contact made by 20 nm Cr/300 nm Au was evaporated on the top of the Bi diodes to protect them. C-V and I-V measurements were carried out at 290 K in a Janis probe station (model CCR10-1) with a Hewlett Packard 4145 Semiconductor Parameter Analyzer and a 4284A LCR meter, respectively.

In order to distinguish between the role of the substrate orientation and the hydrogen blockade on the electrodeposition of the Bi layers [35], we have carried out two different growth procedures. In the first procedure, films are grown by applying a DC potential of -0.2 V. The second procedure consists on the scan route described in ref. 38: a CV of two scans is performed and afterwards the film is grown applying a DC potential of -0.2 V.

Results and Discussion

The two substrates studied in this work, GaAs(110) and (111)B, have different chemical composition and atomic arrangement in the surface. Since they are immersed in an electrolyte, their surface atoms are positioned at bulk-like positions ("truncated" bulk) because dangling bonds are saturated with adsorbed species, inhibiting surface reconstructions [23, 34, 39]. Therefore, the ideal (110) orientation exhibits both Ga and As atoms in a rectangular lattice, with an atom

density of $8.85 \cdot 10^{14}$ cm^{-2} and one dangling bond per atom (Figure 1.a). On the contrary, the (111)B orientation has only As atoms in an hexagonal lattice, with an atom density of $7.22 \cdot 10^{14}$ cm^{-2} and again one dangling bond per atom (Figure 1.c).

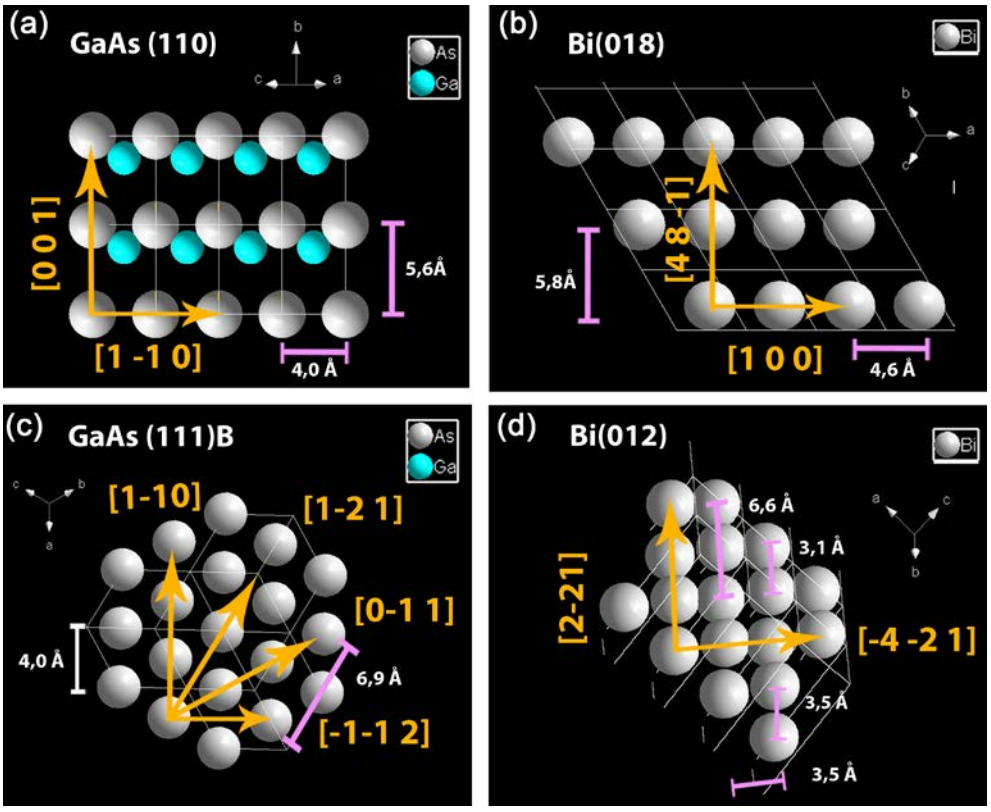

Figure 1. Crystal planes (a) GaAs(110), (b) Bi(018), (c) GaAs(111)B and (d) Bi(012), obtained from the Diamond program and the data in references 36 and 37.

1. Electrochemical behaviour of n-GaAs substrates in the Bi(III) solution

In order to study the effect of the substrate orientation on the electrodeposition of Bi ultra-thin films on n-GaAs electrodes, it is necessary to previously analyze the kinetics of Bi(III) ions on each substrate. CV of two scans were carried out on GaAs(110) and GaAs(111)B with a scan rate of 10 mV/s. CV scans start at the OCP (≈ 70 mV for both substrates) and go towards negative potentials till -0.7 V. Then, the potential is swept to the anodic region being the second reverse potential 0.6 V and eventually, returning back to the OCP. The second scan is performed

just after the first one and it is identical to it. To give further insight into the electrochemical behaviour of each surface, CV scans are represented in a Tafel plot [40] (Figure 2).

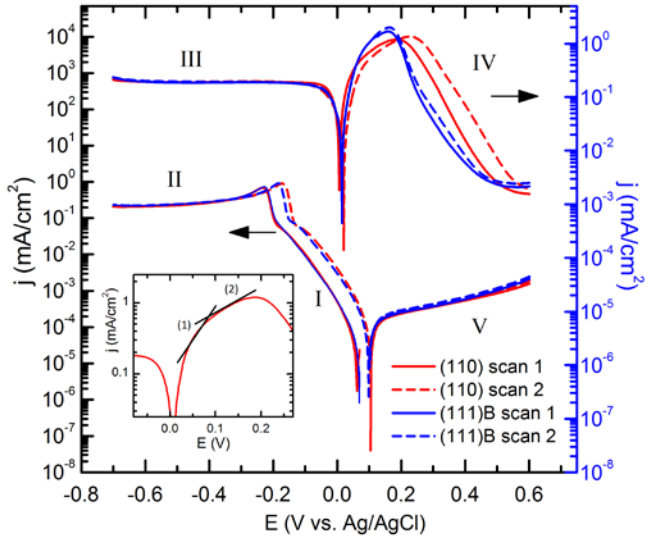

Figure 2. Tafel plot of CV scans performed on n-GaAs(110) and (111)B substrates in the Bi(III) solution. Scan rate of 10 mV/s. The inset is an enlargement of the anodic stage of scan 1 performed on GaAs(110) to show the two slopes of the curve.

The cathodic stage of the CVs (regions I, II and III in Figure 2) are quite similar for both orientations, which indicates that the kinetics of Bi(III) ions is comparable in the two studied surfaces. We can also observe in both orientations some features related to the surface blockade caused by the adsorbed hydrogen (H_{ads}) layer [35]. Firstly, the OCP (minimum delimited by regions I and V) in scan 1 (70 mV) is smaller than the OCP in scan 2 (100 mV) due to the effect of H_{ads} in the potential distribution of the SEI. In the first scan, surface states are passivated by the H_{ads} so surface dipole is changed [34, 41], whereas in the second scan the substrate surface is in intimate contact with the electrolyte [38]. Secondly, the charge transfer resistance obtained from the intersection of the Tafel curve with the vertical line crossing the OCP [42] is higher in scan 1 than in scan 2. Finally, both orientations present a shift between the reduction peak of the first and the

second scan and the onset potential of the first one (defined as the intersection between the rising current and the baseline of the CV) is the same in both surfaces because it corresponds to the onset potential of hydrogen reduction (-196 mV). Hydrogen adsorption seems to be comparable in both orientations, since CV efficiencies are similar in both cases (70 % for scan 1 and 74 % for scan 2). Considering that the H_{ads} is removed after the first scan [38], the onset potential of the reduction peak in the second scan gives information about the electrical activity of each n-GaAs orientation. GaAs(110) exhibits a smaller onset potential (-139 mV) than GaAs(111)B (-155 mV) due to the presence of Ga atoms in the former orientation. These atoms are responsible for lower flat band potentials [43] probably because of the acceptor character of the Ga-derived states [23-24].

The anodic stage (regions IV and V in Figure 2) shows more remarkable differences between the two surfaces. Although the anodic peaks have the same area, i.e. the same amount of Bi is dissolved, the dissolution rate is higher at GaAs(111)B, leading to narrower peaks. Two slopes are observed for each surface orientation (inset of Figure 2) which indicates two different mechanisms involved in the Bi dissolution and related to the electrons transport from the Bi film to the GaAs substrate. At low potentials, electrons cross the Schottky barrier mainly by tunnel effect whereas at higher overpotentials thermionic emission becomes the predominant contribution [29]. Tunnel transport seems similar in both orientations, which means that the depletion region of the Schottky barriers has a similar width. However, the slope at higher potentials, which is linked to thermionic emission, is higher for the (111)B orientation, due to a lower barrier height or to a higher density of surface states at the Bi/GaAs(111)B interface [26].

In order to differentiate between the effect of H_{ads} and the effect of substrate orientation in the electrodeposition of Bi, films with a thickness of 40 nm have been grown in GaAs(110) and

(111)B substrates following the two different procedures already described in the Experimental Methods section. The first procedure (Proc. 1) consists on growing the Bi film by applying a DC potential of -0.2 V so the Bi layer will show effects from both the H_{ads} and the surface orientation. The second procedure (Proc. 2) consists on the scan route described in reference 38 in which a first CV, as shown in Figure 2, is performed in order to unblock the n-GaAs surface and then, a DC potential of -0.2 V is applied to grow the Bi film. By this latter procedure, a Bi layer will be deposited showing only the influence of the substrate orientation. The electrodeposition time for both substrates and both procedures is around 630 seconds.

Figure 3.a shows current-time transients associated to the nucleation process of Bi films deposited on both surface orientations following Proc.1 and Proc. 2. At a very early stage of the growth ($t < 1$ s), the current decreases due to the charging of the double-layer. Afterwards, the current increases as a result of the formation and growth of Bi nuclei on the GaAs. The current reaches a maximum value (j_{max}, t_{max}) and then decreases due to the overlap of the diffusion fields of the growing nuclei and the decrease of the electrode area associated with it.

The transient curves are very similar, and they only reflect differences related to the growth procedure (Figure 3.a). Therefore, the substrate orientation seems to have a lower influence than the H_{ads} on the nucleation. When Proc. 1 is performed, both the induction time (the time to charge the double-layer) and t_{max} increase, whereas j_{max} decreases due to the presence of H_{ads} on the GaAs surface that hinders the Bi growth. When procedure 2 is followed, the current-time transients are similar for both surface orientations except for the higher value of j in the (110) orientation. This could be attributed to a higher density of surface atoms of this surface.

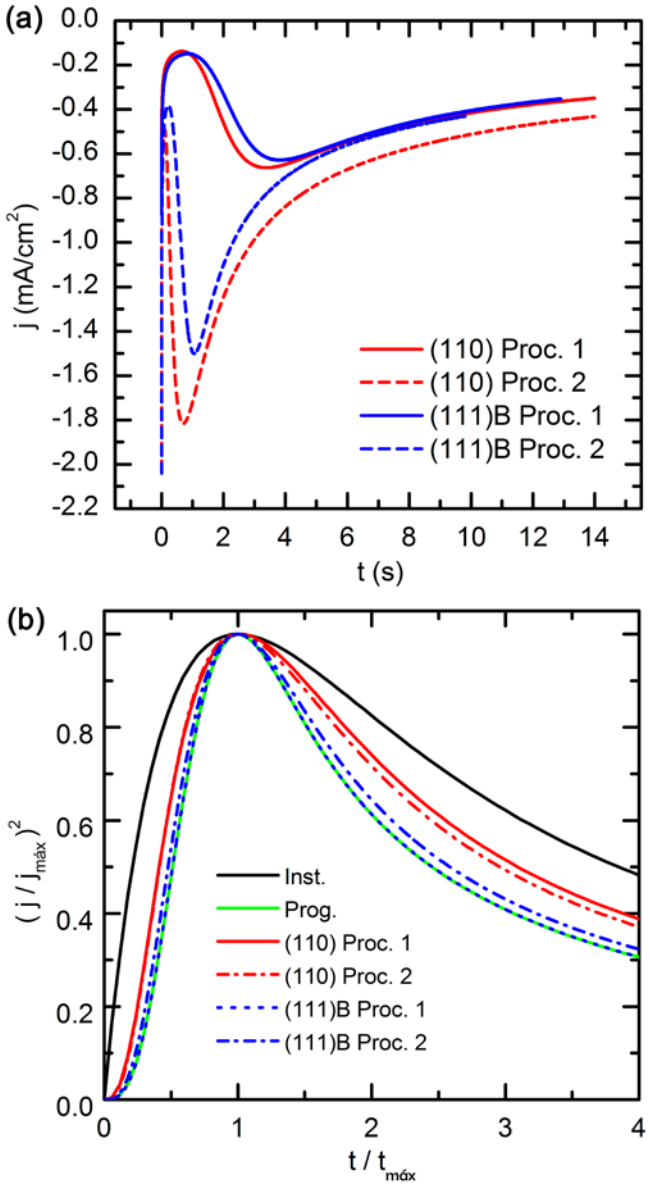

Figure 3. (a) Current-time transients for Bi films grown on n-GaAs substrates (110) and (111)B following the two procedures. (b) Non-dimensional plot of the experimental curves shown in a) and theoretical curves for instantaneous and progressive nucleation.

In order to obtain kinetic information about the nucleation process, the current transients have been analyzed by means of the nucleation model derived by Scharifker and Hills [44]. The experimental transients have been plotted in a non-dimensional form and compared with the theoretical curves for instantaneous (eq. 2) and progressive nucleation (eq. 3) (Figure 3.b).

$$\left(\frac{j}{j_{max}}\right)^2 = \frac{1.9542}{t/t_{max}}\left\{1-\exp\left[-1.2564\cdot\left(\frac{t}{t_{max}}\right)\right]\right\}^2 \quad (2)$$

$$\left(\frac{j}{j_{max}}\right)^2 = \frac{1.2254}{t/t_{max}}\left\{1-\exp\left[-2.3367\cdot\left(\frac{t}{t_{max}}\right)^2\right]\right\}^2 \quad (3)$$

The time scale has been corrected (taken $t = t - t_0$) to avoid the delay effect of the induction time (t_0) [45]. The experimental data can be described by progressive 3D nucleation controlled by diffusion for both substrate orientations, which is the typical nucleation observed when electrodepositing metals onto semiconductors [40]. The adimensional plot of Figure 3.b shows a progressive nucleation for GaAs(111)B and both procedures. However, GaAs(110) shows an intermediate behaviour that can be attributed to the presence of Ga atoms on the surface of that substrate. This behaviour is related to the competition between protons and Bi(III) ions to get adsorbed onto As surface atoms [34, 38], which leads to a progressive nucleation. However, there is no such competition in the case of Ga atoms because protons do not adsorb on them [34]. Therefore, the reduction of Bi(III) ions on GaAs(110) substrates seems to be instantaneous at Ga surface atoms but progressive at As surface atoms. The same explanation has been given by Depestel and Strube to explain the different nucleation mechanism of gold on GaAs(111)A and GaAs(111)B surfaces [24]. From the values of j_{max} and t_{max}, the apparent nucleation rate (AN_0), which is the product of the nucleation rate per active site (A) and the density of active sites (N_0), and the diffusion coefficient of Bi(III) ions (D) have been estimated by means of equations (22) and (23) in reference 44. Table 1 summarizes the values obtained for each procedure and substrate orientation. Proc. 1 provides smaller values of D and AN_0 than Proc. 2 in both surfaces probably because of the distortion that the H_{ads} layer produces in the current transients. Proc. 2 gives nearly the same value of diffusion coefficient in both orientations which is slightly higher

that the values found in the literature [46,47]. The AN_0 values obtained with this procedure are 45 % higher in the (110) orientation than in the (111)B. This difference cannot only be related with the higher surface atom density in the (110) surface (18 % higher) but also to the presence of Ga atoms in this surface.

Orientation	(110)		(111)B	
Procedure	Proc. 1	Proc. 2	Proc. 1	Proc. 2
AN_0 (10^3 cm^{-2} s^{-1})	11	128	9	70
D (10^{-5} cm^2 s^{-1})	1.3	2.3	1.3	2.2

Table 1. Apparent nucleation rate (AN_0) and diffusion coefficient of Bi(III) ions (D) obtained for the two growth procedures and the two substrate orientations.

2. Structural and morphological characterization of Bi ultra-thin films

XRD analysis has been carried out to check the effect of the growth procedure and substrate orientation on the Bi crystallinity. Due to the small thickness of the films, out-of-plane GIXRD patterns have been carried out (Figure 4). All patterns only show a few reflections assigned to the rhombohedral structure of metallic Bi (R-3m, 166), which indicates that all films have a preferred orientation parallel to the substrate surface [48]. The samples grown via procedure 2 present fewer Bragg peaks than those grown via procedure 1, which indicates an enhancement of the crystallinity in the former case.

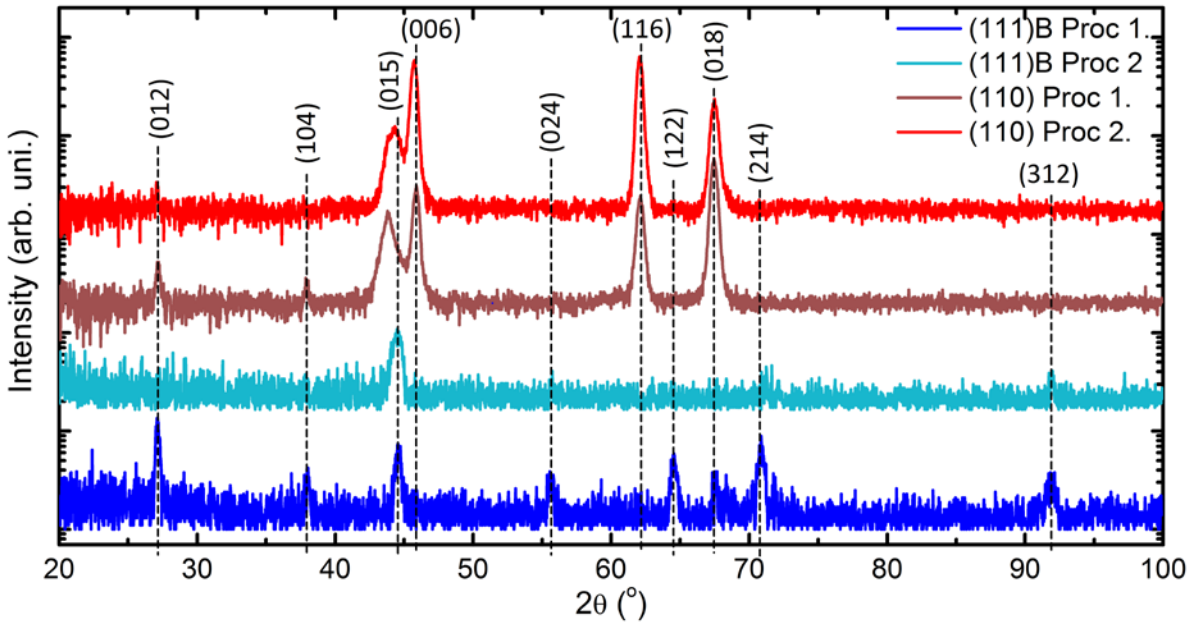

Figure 4. GIXRD patterns of 40nm-Bi thin films grown on GaAs(110) and GaAs(111)B substrates at -0.2V and 300K. The dashed lines indicate the position of Bi reflections (ICDD card 00-044-1246) that matches with an observed peak.

In order to determine the preferred orientation of the Bi layers, symmetric Bragg-Brentano XRD measurements have been carried out (Figure 5). Bi films grown on GaAs(111)B show a (012) texture whereas the films deposited on GaAs(110) present a (018) texture. Other authors have obtained electrodeposited Bi films with the same texture on these GaAs orientations [19, 30-31]. In the case of Bi films grown on GaAs(110) substrates there is also a small contribution of Bi(012) planes when Proc. 1 is followed, which indicates a higher crystal disorder.

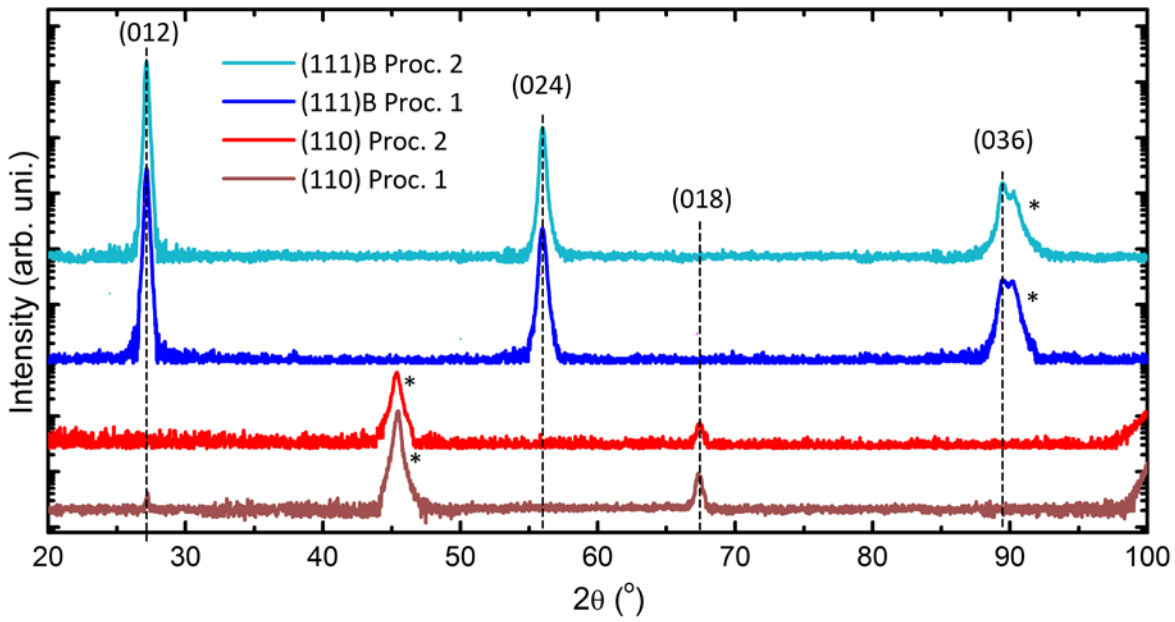

Figure 5. Bragg-Brentano XRD patterns of 40nm-Bi thin films grown on GaAs(110) and GaAs(111)B substrates at -0.2V and 300K. The dashed lines indicate the position of Bi reflections (ICDD card 00-044-1246) that matches with an observed peak. Peaks marked with * correspond to GaAs(110) and GaAs(333) reflections.

We have studied the out-of-plane crystallographic uniformity of the Bi films by means of ω-rocking scans performed around the strongest reflections observed in the symmetric XRD patterns, i.e. Bi(018) and Bi(024) Bragg reflections for Bi on GaAs(110) and (111)B, respectively (Figure 6). It should be pointed out that the Bi(024) reflection has been used instead of the Bi(012) because the GaAs(111) reflection interferes with it. The Bi films grown via Proc. 2 show narrower ω-rocking curves with higher intensity than those grown via Proc. 1. The average tilt (FWHM/2) of Bi(018) and Bi(012) crystallites decreases from 0.3^{o} to 0.25^{o} and from 0.23^{o} to 0.14^{o}, respectively, when Proc. 2 is followed instead of Proc. 1 (Table 2). This indicates a lower crystal quality in the films grown via Proc. 1 because the H_{ads} layer hinders a good nucleation of the Bi layer.

Orientation	(110)		(111)B	
Surface	Proc. 1	Proc. 2	Proc. 1	Proc. 2
Tilt (^{o})	0.30	0.25	0.23	0.14
Twist (^{o})	0.15	0.15	5.80	5.00

Table 2. Tilt and twist average values for Bi films grown on GaAs(110) and (111)B substrates with both growth procedures.

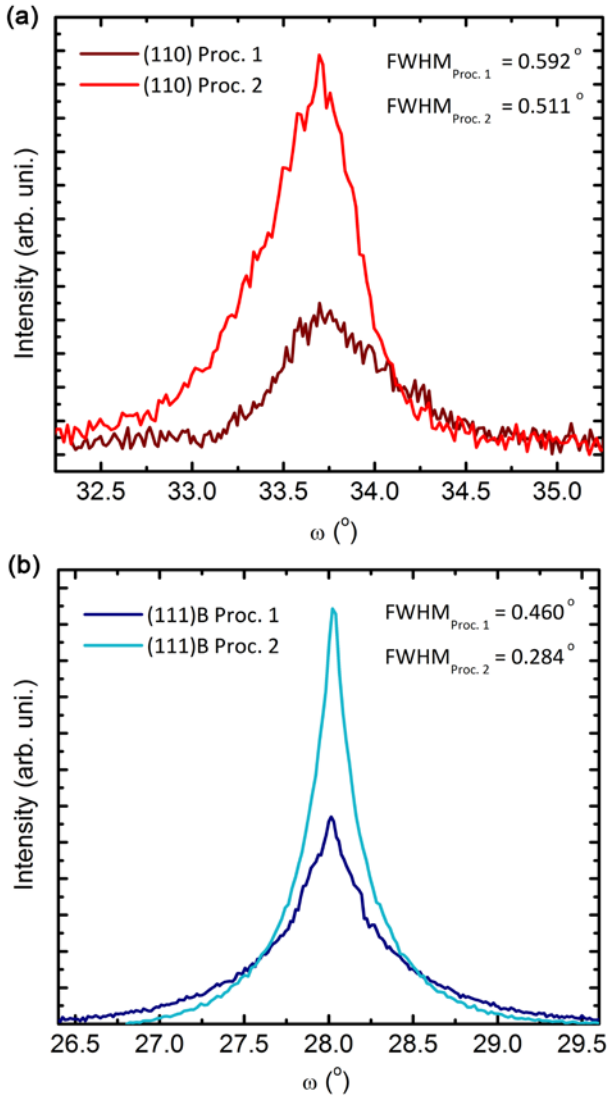

Figure 6. Rocking curves performed on 40 nm-Bi thin films grown on (a) GaAs(110) and (b) GaAs(111)B substrates following the two growth procedures detailed in the text.

The in-plane crystallographic uniformity of the Bi films can be studied by means of φ-scans (azimuthal scans). These measurements are performed around the strongest asymmetric-Bragg reflections, i.e. reflections that are not related to the layer texture. In the case of Bi(018) films grown on GaAs(110), we have chosen Bi(012) and GaAs(200) reflections (Figure 7.a). Both, the substrate and the Bi layer present a two-fold symmetry in agreement with the reflection symmetry, indicative of a single in-plane orientation. An average twist (FWHM/2) of 0.3^{o} has been obtained for both the substrate and the Bi layers grown by the two growth procedures, which indicates a strong in-plane texture with no twist between Bi grains (Table 2), i.e. the Bi(018) plane can form an epitaxial (1x1) layer on GaAs(110). Taking into account the 90^{o} rotation between Bi and GaAs reflections and the rectangular lattice of both Bi(018) and GaAs(110) planes, we inferred an orientation relationship [4 8 $\bar{1}$]Bi || [0 0 1]GaAs and [1 0 0]Bi || [1 $\bar{1}$ 0] GaAs (Figure 1.b). Since each Bi atom in the Bi(018) plane has three dangling bonds and each Ga and As surface atoms in the GaAs(110) plane has one dangling bond, Bi atoms probable make bonds with both As and Ga atoms. Using the values of the bulk material, the vertical directions in Figure 1.a and Figure 1.b have a mismatch of 3%, whereas the horizontal directions present a mismatch of 13%. This result is in agreement with other studies [19, 30-31].

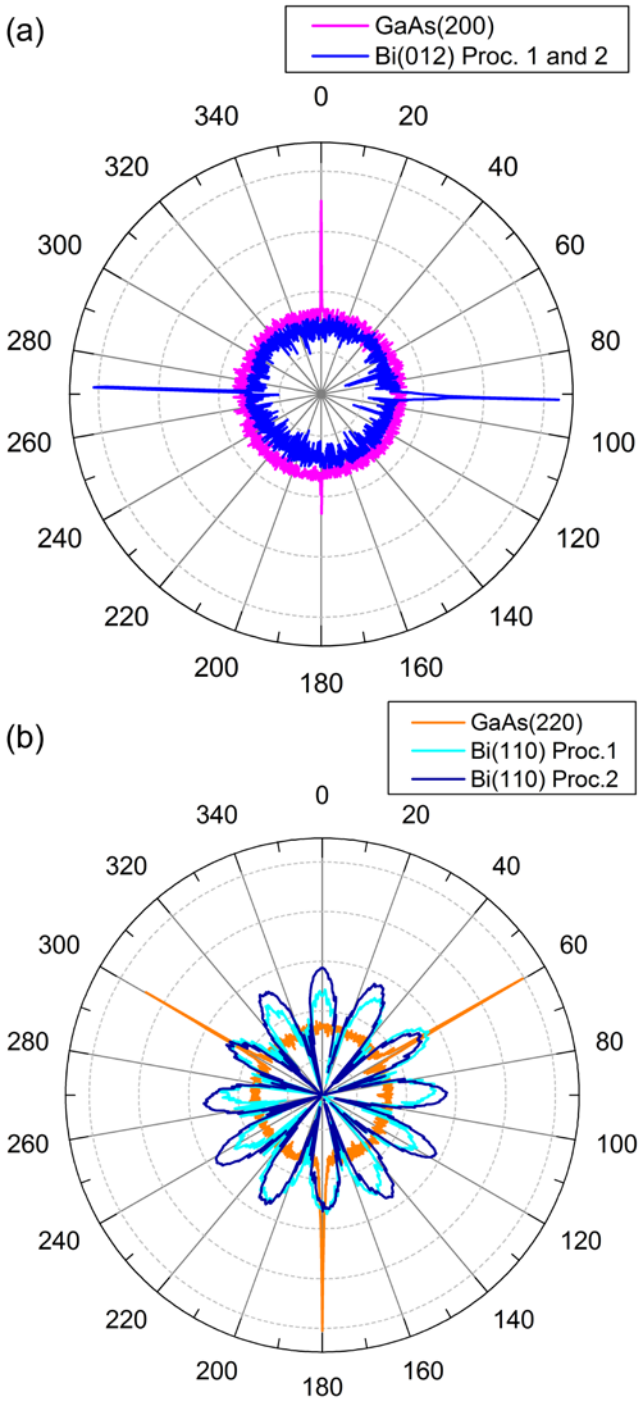

Figure 7. Semilogarithmic polar diagrams of azimuthal scans performed on 40nm-Bi thin films grown on (a) GaAs(110) and (b) GaAs(111)B substrates following the two growth procedures detailed in the text. The curves corresponding to Bi(110) reflection has been rescaled (x4).

In Bi(012) films grown on GaAs(111)B, Bi(110) and GaAs(220) asymmetric-Bragg reflections were selected for φ–scans (Figure 7.b). GaAs(220) shows three reflections in agreement with its three-fold symmetry. Although Bi(110) has also a three-fold symmetry, the azimuthal scan shows 12 reflections. This indicates a complex in-plane arrangement, where Bi grains are distributed in four possible orientations with respect to GaAs(111)B planes and are rotated 30^o between them. Taking into account these angles, we infer that the Bi[$2\bar{2}$ 1] can be parallel to both GaAs[$1\bar{1}$ 0] and GaAs[$0\bar{1}$ 1] directions whereas the Bi[$\bar{4}\bar{2}$ 1] direction can be parallel to both GaAs[$1\bar{2}$ 1] and GaAs [$\bar{1}$ $\bar{1}$ 2] directions (Figure 1.c and d). Using the values of the bulk material, the former directions have a mismatch of 12% or 23% depending on the distance between Bi atoms in the [$2\bar{2}$ 1] direction that can be 3.1 or 3.5 Å, whereas the latter directions present a mismatch of only 5%. These Bi layers have also a considerable mosaicity, since the average twist (FWHM/2) is around 5^o (Table 2). This is a consequence of the 86^o angle between the directions Bi[$2\bar{2}$ 1] and Bi[$\bar{4}\bar{2}$ 1], which have to fit with the directions GaAs[$1\bar{1}$ 0] and GaAs[$\bar{1}\bar{1}$ 2], respectively, which form an angle of 90^o. This misfit enables the Bi(012) grains to twist $\pm 4^o$ around the above mentioned GaAs directions, leading to the mosaicity observed. In addition, when the H_{ads} layer is present at the beginning of the Bi film growth (Proc. 1) the mosaicity is higher (5.8^o) than when it is not (Proc. 2, 5^o). Therefore, we can conclude that a better crystallinity is obtained when Bi films are grown via procedure 2, as a result of the better nucleation for the lower misfit.

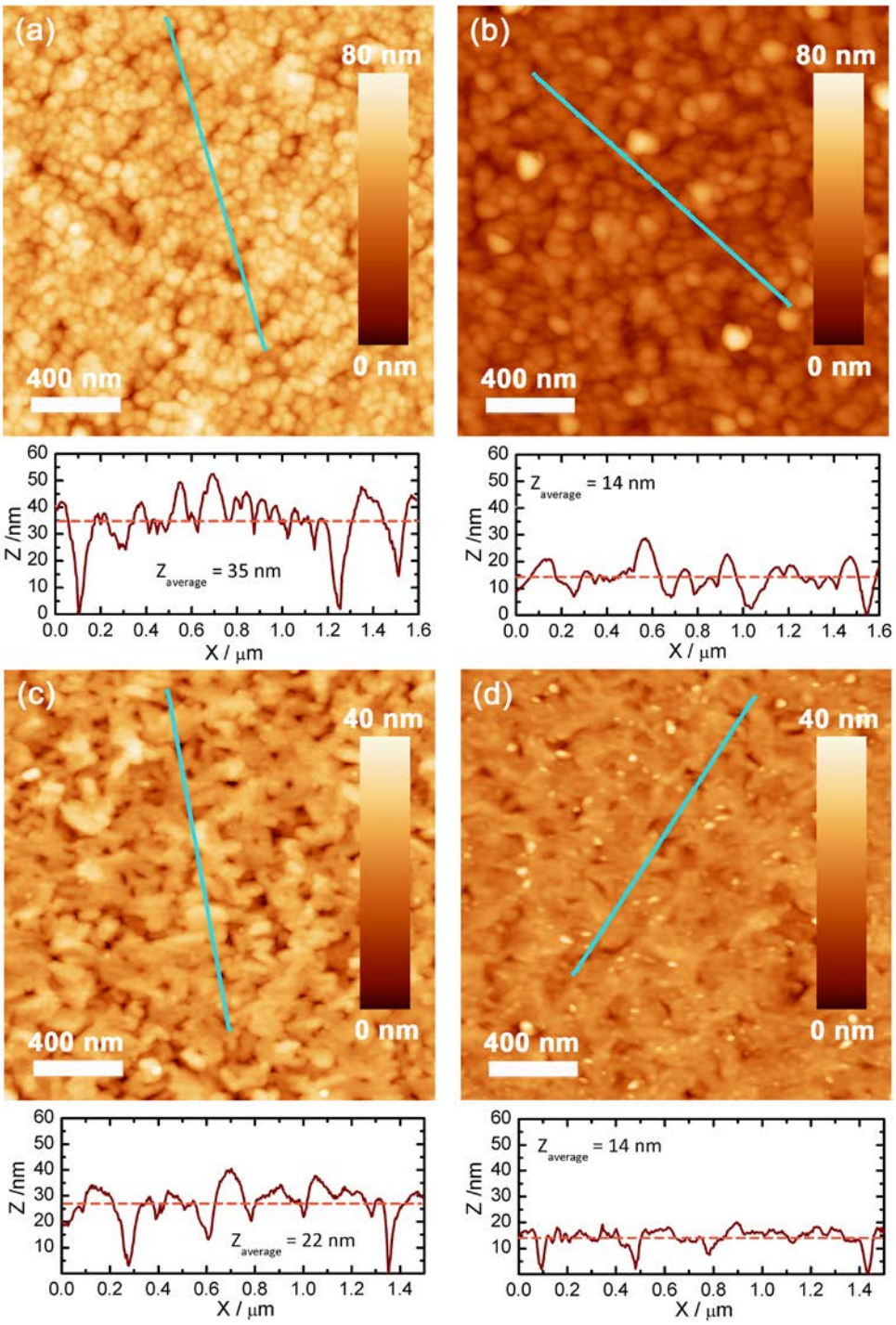

Figure 8. AFM images of 40 nm Bi thin films grown on GaAs(110) and GaAs(111)B substrates at -0.2V and 300K. (a) and (c) show films grown following procedure 1. (b) and (d) show films grown following procedure 2.

All Bi films exhibit a surface morphology in agreement with a 3D nucleation as expected by current-time transients (Figure 8). AFM images show that, in general terms, the morphology of the Bi layers is dependent on the substrate orientation regardless of the growth procedure. Bi layers grown on GaAs(111)B substrates present elongated islands and a small roughness, in agreement with the higher out-of-plane crystal uniformity. The flatter Bi surface when using GaAs(111)B as a substrate is also in agreement with the progressive nucleation obtained for that orientation However, Bi layers grown on GaAs(110) substrates exhibit rounded islands with a higher roughness, as a result of the higher average tilt of the Bi(018) crystallites. The higher rms in this case is also in agreement with the mixed character of the nucleation, progressive plus instantaneous. For both substrate orientations, depth profiles show that the Bi films grown via Proc. 2 are more compact than those grown via Proc. 1. Depth profiles show the existence of some areas of the substrate that are not well covered as a result of the H_{ads} in the Bi layers grown via Proc.1 [38]. In addition to the higher compactness, Proc. 2 provides flatter Bi films decreasing the rms between 12-20% (Table 3).

Orientation	(110)		(111)B	
Surface	Proc. 1	Proc. 2	Proc. 1	Proc. 2
rms (nm)	7.3	5.8	4.1	3.6
Average island size (nm)	50	85	50	55

Table 3. rms and average island size values inferred from AFM images for 40 nm Bi films grown on GaAs(110) and GaAs(111)B substrates.

3. Electrical properties of Bi/n-GaAs interfaces

To conclude this study, Bi/GaAs diodes have been fabricated to electrically characterize the Bi/GaAs interface. C-V as well as I-V curves have been measured at 290 K as a function of substrate orientation and growth procedure. Firstly, C-V curves have been measured on Au/Cr/GaAs Schottky diodes to estimate the electron concentration of the GaAs substrates. The resulting values were $9.5 \cdot 10^{17} cm^{-3}$ for (110) and $8.5 \cdot 10^{17} cm^{-3}$ for (111)B in perfect agreement with the wafers specifications. Since $n > N_c$, where n is the electron concentration and N_c (= $4.7 \cdot 10^{17}$ cm^{-3}) is the effective density of states for electrons in the conduction band [37], our substrates are degenerate.

Afterwards, C-V curves have been carried out on Bi/GaAs diodes for both substrate orientations and growth procedures. In Figure 9.a it is shown the C^{-2}-V curves studied for all the samples.

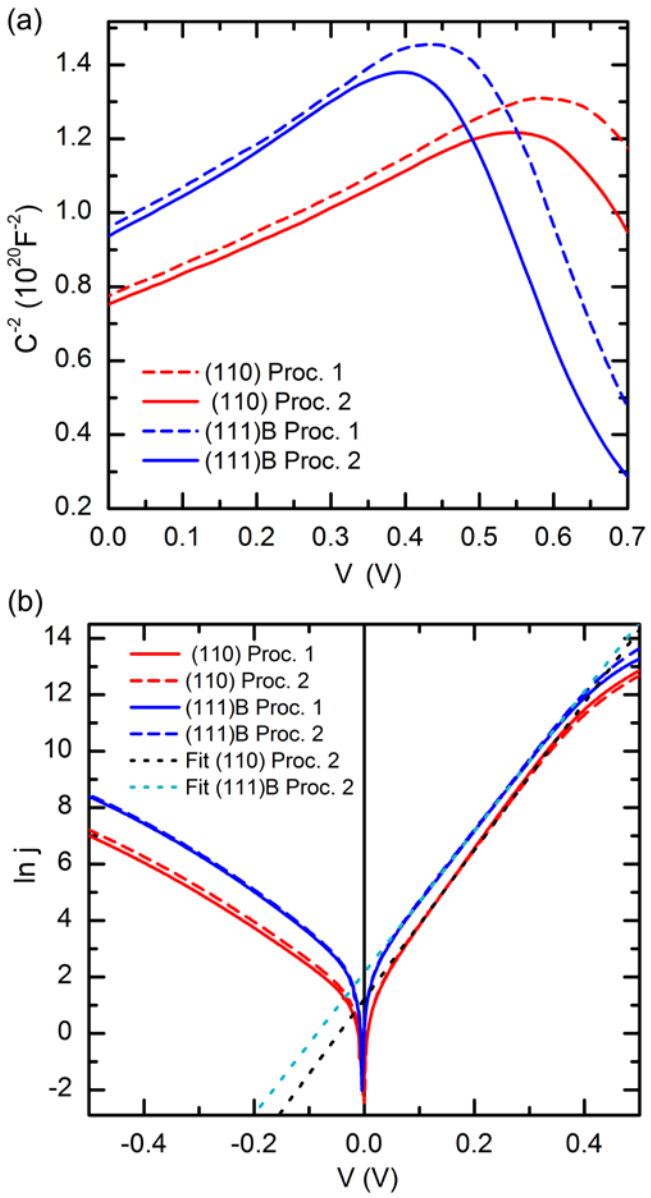

Figure 9. (a) C^{-2}-V curves and (b) ln j -V curves of Bi/GaAs diodes as a function of substrate orientation and growth procedure.

To infer the flat band potential (ϕ_{FB}) from the intercept (V_0) of the C^{-2} curve with the voltage axis, an important correction should be made according to the Goodman and Perkins model [49] derived for the differential capacitance of a metal contact to a degenerate semiconductor.

$$\phi_{FB} = V_o + K\frac{kT}{q} \tag{4}$$

where

$$K = \ln\left[1 + 2\exp(\varepsilon_D + \eta)\right] + \frac{\frac{2}{3}\cdot F_{3/2}(\eta)}{\left[1 + 2\exp(\varepsilon_D + \eta)\right]\cdot F_{1/2}(\eta)} \quad (5)$$

where η is the reduced Fermi level with respect to the bottom of the conduction band, ε_D is the reduced donor energy level respect to the bottom of the conduction band, $F_j(\eta)$ are the Fermi integrals [50], k is the Boltzmann constant, T is the temperature and q is the electron charge. The calculation of η and ε_D energy levels is derived from the experimental value of n previously obtained and it is detailed in the appendix. From the flat band potential and the position of the Fermi level, the barrier height (ϕ_B) can be derived as:

$$q\phi_B = q\phi_{FB} - \eta\cdot kT = q\phi_{FB} - \left(E_F - E_C\right) \quad (6)$$

Table 4 summarizes the values of the (E_F - E_C), ϕ_{FB} and ϕ_B for the Bi/GaAs interfaces for both substrate orientations and growth procedures. Bi films grown via Proc. 1 have barrier heights higher (2-3%) than those grown via Proc. 2 regardless of the substrate orientation (table 4). Since these layers have been grown onto hydrogenated GaAs surfaces, this increase in the barrier height is due to the presence of H_{ads} trapped in the Bi/GaAs interface. The hydrogen atoms passivate the surface states at the interface, enhancing the surface dipole of the Bi and, therefore, leading to a higher effective barrier height [51-52]. Furthermore, the Bi layers grown on GaAs (110) present a higher barrier height (~ 60 meV) than those obtained in GaAs(111)B, probably due to the enhanced in-plane crystal uniformity. On the contrary, the high mosaicity of the Bi films grown on GaAs(111)B leads to a large density of grain boundaries and, therefore, to surface states that decrease the barrier height. This result is in agreement with the faster Bi dissolution observed for GaAs(111)B substrates at the electrochemical characterization (Figure 2).

Figure 9.b shows the semilogarithmic I-V characteristics of a metal-semiconductor junction with excess current at the reverse bias which indicates tunnel transport through the Schottky barrier. It is known that GaAs substrates with a doping level $N_D > 1 \cdot 10^{17}$ cm^{-3} exhibit sufficiently thin barriers at 300 K to allow electrons tunneling from the conduction band to the metal [53]. Therefore, I-V characteristics should be analyzed on the basis of Thermionic Field Emission (TFE) [54]. The forward current (j_n) can be described by the following relation:

$$j_n = j_S \cdot \exp\left(\frac{E}{E_0}\right) \tag{7}$$

where

$$j_S = \frac{A^* T^2 \left[\pi \cdot E_{00} \cdot \left(q\phi_B - E + \xi\right)\right]^{\frac{1}{2}}}{kT \cdot \cosh\left(E_{00} \big/ kT\right)} \cdot \exp\left(\frac{\eta}{kT} - \frac{q\phi_B + \xi}{E_0}\right) \tag{8}$$

Here j_s is the saturation current, E is the potential energy associated with the applied bias (V) between the metal and the semiconductor, ξ is the Fermi energy measured with respect to the bottom of the conduction band and A^* is the Richardson constant. The energy E_0 is given by:

$$E_0 = E_{00} \cdot \coth\left(\frac{E_{00}}{kT}\right) \tag{9}$$

where

$$E_{00} = \frac{q \cdot h}{4\pi} \cdot \left(\frac{N}{m_t \cdot \varepsilon}\right)^{\frac{1}{2}} \tag{10}$$

Here h is Planck constant, N is the ionized donor concentration (equal to the electron concentration, n), m_t is the tunneling mass for the electrons measured in the unit of the free electron mass and ε is the semiconductor permittivity.

The experimental characteristics shown in Figure 9.b have been analyzed by a non-linear fitting of equation 7 to the experimental data using the Marquardt–Levenberg algorithm. The m_t has been set as a free parameter as well as ϕ_B, because it can be affected by the crystal disorder at the interface [18]. Therefore, equation 7 can be written as the following equation (the detailed calculation is given in the appendix):

$$\ln j_n = \ln A + B \tag{11}$$

where

$$A = \frac{5.1285 \cdot 10^5 \cdot N^{1/4} \cdot m_t^{3/4}}{\cosh\left(2.0278 \cdot 10^{-12} \cdot \frac{N^{1/2}}{m_t^{1/2}}\right)} \cdot \left(q\phi_B - E + \xi\right)^{\frac{1}{2}} \tag{12}$$

$$B = \frac{\eta}{0.025} - \frac{\left(q\phi_B - E + \xi\right)}{\left(5.137 \cdot 10^{-15} \cdot \frac{N^{1/2}}{m_t^{1/2}}\right) \cdot \coth\left(2.0278 \cdot 10^{-12} \cdot \frac{N^{1/2}}{m_t^{1/2}}\right)} \tag{13}$$

The best-fit parameters from at least 10 different diodes were averaged to give the values listed in Table 4. Just as in the C-V curves, the barrier heights obtained by the I-V curves are a little higher in the (110) orientation. In addition, Bi/GaAs diodes obtained by Proc. 1 present barrier heights slightly lower than those obtained by Proc. 2. This might be related to a higher oxidation of the diode due to the higher rms of the Bi films grown by Proc. 1 [55]. In all cases, the m_t obtained is smaller than the electrons mass in GaAs which indicates crystal defects at the interface. The (111)B orientation shows the lowest values of m_t due to the high mosaicity of the Bi layers grown on this orientation. On the contrary, the Bi layers grown on GaAs(110) have a negligible mosaicity but a higher out-of-plane disorder, which leads also to a small value of m_t.

Orientation	(110)		(111)B	
Procedure	Proc. 1	Proc. 2	Proc. 1	Proc. 2
E_F - E_C (meV)	40.7	40.7	36.0	36.0
$q{\cdot}\phi_{FB}$ (eV)	0.913	0.885	0.835	0.816
$q{\cdot}\phi_B^{CV}$ (eV)	0.863	0.833	0.796	0.780
$q{\cdot}\phi_B^{IV}$ (eV)	0.842	0.854	0.835	0.837
m_t	0.0267	0.0237	0.0203	0.0198

Table 4. Fermi level position with respect to the conduction band edge (E_F - E_C), flat band potential ($q{\cdot}\phi_{FB}$) and barrier height inferred from C-V curves ($q{\cdot}\phi_B^{CV}$). Barrier height ($q{\cdot}\phi_B^{IV}$) and tunneling mass (m_t) derived from I-V curves.

The barrier heights obtained by both C-V and I-V measurements for the Bi films grown on GaAs(110) are comparable to literature values [19]. However, Bi films grown on GaAs(111)B present higher barrier heights than those obtained by other authors [19, 30]. C-V and I-V curves provide different values for the barrier height mainly due to two effects. On one hand, I-V curves measure the electrons transport through the Schottky barrier which is affected by image forces and contact resistances, whereas C-V curves measure capacitive effects. On the other hand, when an interface is not completely abrupt there is a barrier height fluctuation at the interface that distorts I-V curves from the theoretical models which suppose uniform and abrupt barriers with a fixed value for the barrier height. However, C-V curves performed on non uniform interfaces only give an average value of the barrier height. Therefore, C-V measurements usually give more reliable values of the Schottky barrier height than I-V measurements.

Conclusions

The effect of n-GaAs surface orientation on the electrodeposition of 40 nm Bi layers has been studied by means of different techniques. Firstly, cyclic voltammetries and transient curves have been used to observe the electrochemical properties of (110) and (111)B GaAs surface orientations. Afterwards, the crystal structure and morphology of Bi films grown by different procedures have been determined by XRD analysis and AFM images. Finally, the Bi/GaAs interface has been characterized by C-V and I-V curves. In this study, we have been able to differentiate between the effect of surface atomic arrangement and the surface chemical composition of GaAs substrates. The former determines the crystal structure of the Bi layers, as well as their surface morphology. The latter influences on the electrochemical properties of the GaAs electrodes and on the electrical properties of the Bi/GaAs interface. Finally, we have observed the effect of the H_{ads} layer on the electrochemical properties of the GaAs electrodes, and on the structural, and morphological properties of Bi layers as well as the electrical properties of Bi/GaAs interfaces. The H_{ads} layer passivates the GaAs surface distorting its electrochemical behaviour. In addition, the H_{ads} hinders Bi(III) ions reduction which is observed as a delay and a decrease of current density in current transients. Regardless of substrate orientation, Bi layers grown without removing the H_{ads} layer show a higher roughness and a lower crystal quality than those obtained after removing the H_{ads}. Finally, the effect of the H_{ads} in the two orientations is to enhance the Schottky barrier height because the hydrogen trapped at the Bi/GaAs interface passivates surface states, increasing Bi surface dipole.

APPENDIX

Calculation of the Fermi level

In the bulk of the n-type semiconductor charge neutrality must exist:

$$n = N_D^+ + p$$

Since n > N_C (with $N_C = 4.12 \cdot 10^{17}$ cm^{-3} being the effective density of states for electrons in the conduction band of GaAs at 290 K [37]) the substrates are degenerate. Therefore, electrons concentration has to be described by Fermi-Dirac distribution and holes population can be neglected.

$$N_D^+ \approx n = N_C \cdot F_{\frac{1}{2}}(\eta)$$

According to Nilsson approximation [50], the reduced Fermi position is given by:

$$\eta = \frac{E_F - E_C}{kT} = \frac{\ln u}{1-u^2} + \frac{\left(\frac{3}{4}\sqrt{\pi}\cdot u\right)^{\frac{2}{3}}}{1+\left[0.24+1.08\cdot\left(\frac{3}{4}\sqrt{\pi}\cdot u\right)^{\frac{2}{3}}\right]^{-2}}$$

where

$$u = F_{\frac{1}{2}}(\eta) = \frac{n}{N_C}$$

Calculation of donors energy level

The reduced energy level of donor impurities is defined as:

$$\varepsilon_D = \frac{E_D - E_C}{kT}$$

where E_D is the ionization energy for the donor impurity. The simplest calculation of impurity energy levels is based on the hydrogen-atom model [37]. E_D can be obtained by replacing m_0 and ε_0

by the conductivity effective mass of electrons (m^*) and the semiconductor permittivity (ε_s) in the ionization energy for a hydrogen atom.

$$E_D = \left(\frac{\varepsilon_0}{\varepsilon_s}\right)^2 \left(\frac{m^*}{m_0}\right) \cdot E_H = \frac{0.067}{13.1^2} \cdot 13.6 = 5.3 \cdot meV$$

This result is in good agreement with the activation energy of donor-type Si impurities located in substitutional Ga sites in the GaAs lattice (6 meV) [56].

Derivation of equations 11 and 12

Neperian logarithm of equation 6 is given by equation 10:

$$\ln j_n = \ln A + B$$

where

$$A = \frac{A^* \cdot T^2 \cdot \pi^{1/2} \cdot E_{00}^{1/2}}{kT \cdot \cosh\left(E_{00}/kT\right)} \cdot \left(q\phi_B - E + \xi\right)^{\frac{1}{2}}$$

$$B = \frac{\xi}{kT} - \frac{\left(q\phi_B - E + \xi\right)}{E_0}$$

Substituting the expressions of A^*, E_0 and E_{00}:

$$A = \frac{120 \cdot m_t \cdot T^2 \cdot \left(\frac{qhN^{1/2}}{4\varepsilon^{1/2} m_t^{1/2}}\right)^{\frac{1}{2}}}{kT \cdot \cosh\left(\frac{qhN^{1/2}}{4\pi \cdot \varepsilon^{1/2} m_t^{1/2} kT}\right)} \cdot \left(q\phi_B - E + \xi\right)^{\frac{1}{2}}$$

$$B = \frac{\xi}{kT} - \frac{\left(q\phi_B - E + \xi\right)}{\left(\frac{qhN^{1/2}}{4\pi\varepsilon^{1/2} m_t^{1/2}}\right) \cdot \coth\left(\frac{qhN^{1/2}}{4\pi\varepsilon^{1/2} m_t^{1/2} kT}\right)} \xi$$

Substituting the known values,

$$A = \frac{5.1285 \cdot 10^{5} \cdot N^{1/4} \cdot m_t^{3/4}}{\cosh\left(2.0278 \cdot 10^{-12} \cdot \frac{N^{1/2}}{m_t^{1/2}}\right)} \cdot \left(q\phi_B - E + \xi\right)^{\frac{1}{2}}$$

$$B = \frac{\xi}{0.025} - \frac{\left(q\phi_B - E + \xi\right)}{\left(5.137 \cdot 10^{-15} \cdot \frac{N^{1/2}}{m_t^{1/2}}\right) \cdot \coth\left(2.0278 \cdot 10^{-12} \cdot \frac{N^{1/2}}{m_t^{1/2}}\right)}$$

AUTHOR INFORMATION

Corresponding Author

*rociran@ucm.es

Phone: (+34) 91 394 5012; Fax: (+34) 91 394 4547

Author Contributions

The manuscript was written through contributions of all authors. All authors have given approval to the final version of the manuscript.

Funding Sources

Spanish Ministry of Economy and Competitiveness (projects MAT2014-52477-C5-2-P and MAT2015-66888-C3-3R) Spanish Ministry of Education, Culture and Sport (FPU program, FPU12/04292).

Acknowledgments

We acknowledge partial financial support of this work by Spanish Ministry of Economy and Competitiveness (projects MAT2014-52477-C5-2-P and MAT2015-66888-C3-3R) and Instituto de Sistemas Optoelectrónicos y Microelectrónica (ISOM) facilities. Alicia Prados acknowledge

financial support from Spanish Ministry of Education, Culture and Sport (FPU12/04292) and useful discussions on XRD measurements with I. Carabias and A. Migliorini.

REFERENCES

1. Hirahara, T.; Miyamoto, K.; Kimura, A.; Niinuma, Y.; Bihlmayer, G.; Chulkov, E. V.; Nagao, T.; Matsuda, I. ; Quiao, S.; Shimada, K.; et al. Origin of the Surface-State Band-Splitting in Ultrathin Bi Films: from Rasbha Effect to a Parity Effect. *New J. Phys.* **2008**, *10*, 083038. DOI: 10.1088/1367-2630/10/8/083038.

2. Wada, M.; Murakami, S.; Freimuth, F.; Bihlmayer, G. Localized Edge States in Two-Dimensional Topological Insulators: Ultrathin Bi Films. *Phys. Rev. B* **2011**, *83*, 121310(R). DOI: 10.1103/PhysRevB.83.121310.

3. Yang, F. Y.; Lui, K.; Hong, K.; Reich, D. H.; Searson, P. C.; Chien, C. L.; Leprince-Wang, Y.; Yu-Zhang, K.; Han, K. Shubnikov-de Haas Oscillations in Electrodeposited Single-Crystal Bismuth Films. *Phys. Rev. B* **2000**, *61*, 6631-6636. DOI: 10.1103/PhysRevB.61.6631.

4. Hoffman, C. A.; Meyer, J. R.; Bartoli, F. J.; Venere, A. D.; Yi, X. J.; Hou, C. L.; Wang, H. C.; Ketterson, J. B.; Wong, G. K. Semimetal-to-Semiconductor Transition in Bismuth Thin Films. *Phys. Rev. B* **1993**, *48*, 11431-11434. DOI: 10.1103/PhysRevB.48.11431.

5. Smith, G. Anomalous Skin Effect in Bismuth. *Phys. Rev.* **1959**, *115*, 1561-1568. DOI: 10.1103/PhysRev.115.1561.

6. Isaacson, R. T.; Williams, G. A. Alfvén-Wave Propagation in Solid-State Plasmas. III. Quantum Oscillations of the Fermi Surface of Bismuth. *Phys. Rev.* **1969**, *185*, 682-688. DOI: 10.1103/PhysRev.185.682.

7. Gonze, X.; Michenaud, J.-P.; Vigneron, J.-P. Ab Initio Calculations of Bismuth Properties, Including Spin-Orbit Coupling. *Phys. Scr.* **1988**, *37*, 785-789. DOI: 10.1088/0031-8949/37/5/022.

8. Issi, J. P. Low Temperature Transport Properties of the Group V Semimetals. *Aust. J. Phys.* **1979**, *32*, 585-628. DOI: 10.1071/PH790585.

9. Hartman, R. Temperature Dependence of the Low-Field Galvanomagnetic Coefficients of Bismuth. *Phys. Rev.* **1969**, *181*, 1070-1086. DOI: 10.1103/PhysRev.181.1070.

10. Smith, G. E.; Baraff, G. A.; Rowell, J. M. Effective g Factor of Electrons and Holes in Bismuth. *Phys. Rev.* **1964**, *135*, A1118-A1124. DOI: 10.1103/PhysRev.135.A1118.

11. Murata, M.; Nakamura, D.; Hasegawa, Y.; Komine, T.; Taguchi, T.; Nakamura, S.; Jaworski, C. M.; Jovovic, V.; Heremans, J. Mean Free Path Limitation of Thermoelectric Properties of Bismuth Nanowires. *J. Appl. Phys.* **2009**, *105*, 113706. DOI: 10.1063/1.3131842.

12. Reneker, R. New Oscillatory Absorption of Ultrasonic Waves in Bismuth in a Magnetic Field. *Phys. Rev. Lett.* **1958**, *1*, 440-442. DOI: 10.1103/PhysRevLett.1.440.

13. Hirahara, T.; Miyamoto, K.; Matsuda, I.; Kadono, T.; Kimura, A.; Nagao, T.; Bihlmayer, G.; Chulkov, E. V.; Qiao, S.; Shimada, K.; et al. Direct Observation of Spin Splitting in Bismuth Surface States. *Phys.Rev. B* **2007**, *76*, 153305. DOI: 10.1103/PhysRevB.76.153305.

14. Khvalkovskiy, A. V.; Cros, V.; Apalkov, D.; Nikitin, V.; Krounbi, M.; Zvezdin, K. A.; Anane, A.; Grollier, J.; Fert, A. Matching Domain Wall Configuration and Spin-Orbit Torques for Efficient Domain-Wall Motion. *Phys. Rev. B* **2013**, *87*, 020402(R). DOI: 10.1103/PhysRevB.87.020402.

15. Rojas Sánchez, J. C.; Vila, L.; Desfonds, G.; Gambarelli, S.; Attane, J. P.; De Teresa, J. M.; Magén, C.; Fert, A. Spin-to-Charge Conversion Using Rashba Coupling at the Interface Between Non-Magnetic Materials. *Nat. Commun.* **2013**, *4*, 2944. DOI: 10.1038/ncomms3944.

16. Liu, K.; Chien, C. L.; Searson, P. C. Finite-Size Effects in Bismuth Nanowires. *Phys. Rev. B* **1998**, *58*, R14681 - R14684. DOI: 10.1103/PhysRevB.58.R14681.

17. Cornelius, T. W.; Toimil-Molares, M. E.; Karim, S.; Neumann, R. Oscillations of Electrical Conductivity in Single Bismuth Nanowires. *Phys. Rev. B* **2008**, *77*, 125425. DOI: 10.1103/PhysRevB.77.125425.

18. Kiziroglou, M. E.; Li, X.; Zhukov, A. A.; de Groot; P. A. J.; de Groot, C. H. Thermionic Field Emission at Electrodeposited Ni–Si Schottky Barriers. *Solid-State Electron.* **2008**, *52*, 1032-1038. DOI: 10.1016/j.sse.2008.03.002.

19. Bao, Z. L.; Kavanagh, K. L. Epitaxial Bi/GaAs Diodes Via Electrodeposition. *J. Vac. Sci. Technol. B* **2006**, *24*, 2138-2143. DOI: 10.1116/1.2218874.

20. Vereecken, P. M.; Searson, P. C. Electrochemical Formation of GaAs/Bi Schottky Barriers. *Appl. Phys. Lett.* **1999**, *75*, 3135-3137. DOI: 10.1063/1.125255.

21. Yang, F. Y.; Liu, K.; Hong, K.; Reich, D. H.; Searson, P. C.; Chien, C. L. Large Magnetorresistance of Electrodeposited Single-Crystal Bismuth Thin Films. *Science* **1999**, *284*, 1335-1337. DOI: 10.1126/science.284.5418.1335.

22. Sandnes, E.; Williams, M. E.; Bertocci, U.; Vaudin, M. D.; Stafford, G. R. Electrodeposition of Bismuth From Nitric Acid Electrolyte. *Electrochim. Acta* **2007**, *52*, 6221–6228. DOI: 10.1016/j.electacta.2007.04.002.

23. Lüth, H. *Surface and Interfaces of Solid Materials*; Springer Berlin Heidelberg, Berlin, Germany, 1995. DOI: 10.1007/978-3-662-03132-2.

24. Depestel, L. M.; Strubbe, K. Influence of the Crystal Orientation on the Electrochemical Behaviour of n-GaAs in Au(I)-Containing Solutions. *Phys. Chem. Chem. Phys.* **2003**, *5*, 2881-2885. DOI: 10.1039/B302243A.

25. Bartolomé, J.; Maestre, D.; Cremades, A.; Amatti, M.; Piqueras, J. Composition-Dependent Electronic Properties of Indium–Zinc–Oxide Elongated Microstructures. *Acta Mater.* **2013**, *61*, 1932–1943. DOI: 10.1016/j.actamat.2012.12.014.

26. Miller, E. A.; Richmond, G. L. Photocorrosion of n-GaAs and Passivation by Na_2S: A Comparison of the (100), (110), and (111)B Faces. *J. Phys. Chem. B* **1997**, *101*, 2669–2677. DOI: 10.1021/jp962852k.

27. De Vrieze, A.; Strubbe, K.; Gomes, W. P.; Forment, S.; Van Meirhaeghe, R. L. Electrochemical Formation and Properties of n-GaAs/Au and n-GaAs/Ag Schottky Barriers: Influence of Surface Composition Upon the Barrier Height. *Phys. Chem. Chem. Phys.* **2001**, *3*, 5297-5303. DOI: 10.1039/b104887m.

28. Depestel, L. M.; Strubbe, K. Electrodeposition of Gold From Cyanide Solutions on Different n-GaAs Crystal Faces. *J. Electroanal. Chem.* **2004**, *572*, 195–201. DOI: 10.1016/j.jelechem.2004.06.012.

29. Vereecken, P. M.; Searson, P. C. Electrochemical Deposition of Bi on GaAs (100). *J. Electrochem. Soc.* **2001**, *148*, C733-C739. DOI: 10.1149/1.1406493.

30. Vereecken, P. M.; Rodbell, K.; Ji, C.; Searson, P. C. Electrodeposition of Bismuth Thin Films on n-GaAs (110). *Appl. Phys. Lett.* **2005**, *86*, 121916. DOI: 10.1063/1.1886248g.

31. Plaza, M.; Abuín, M.; Mascaraque, A.; González-Barrio, M. A.; Pérez, L. Epitaxial Growth of Bi Ultra-Thin Films on GaAs by Electrodeposition. *Mater. Chem. Phys.* **2012**, *134*, 523-530. DOI: 10.1016/j.matchemphys.2012.03.027.

32. Mayer, T.; Lebedev, M.; Hunger, R.; Jaegermann, W. Elementary Processes at Semiconductor/Electrolyte Interfaces: Perspectives and Limits of Electron Spectroscopy. *Appl. Surf. Sci.* **2005**, *252*, 31-42. DOI: 10.1016/j.apsusc.2005.01.110.

33. Lebedev, M. V.; Masuda, T.; Uosaki, K. Charge Transport at the Interface of n-GaAs (100) With an Aqueous HCl Solution: Electrochemical Impedance Spectroscopy Study. *Semiconductors* **2012**, *46*, 471-477. DOI: 10.1134/S1063782612040136.

34. Erné, B. H.; Ozanam, F.; Chazalviel, J. -N. Dynamics of Hydrogen Adsorption on GaAs Electrodes. *Phys. Rev. Lett.* **1998**, *80*, 4337-4340. DOI: 10.1103/PhysRevLett.80.4337.

35. Prados, A.; Ranchal, R.; Pérez, L. Blocking Effect in the Electrodeposition of Bi on n-GaAs in Acidic Electrolytes. *Electrochim. Acta* **2014**, *143*, 23-28. DOI: 10/1016.j.electacta.2014.07.137.

36. Cucka, P.; Barrett, C. S. The Crystal Structure of Bi and of Solid Solutions of Pb, Sn, Sb and Te in Bi. *Acta Crystallogr.* **1962**, *15*, 865-872. DOI: 10.1107/S0365110X62002297.

37. Sze, S. M. *Physics of Semiconductor Devices*; John Wiley & Sons, Inc.: New York, USA, 1981. DOI: 10.1002/0470068329.

38. Prados, A.; Ranchal, R.; Pérez, L. Strategies to Unblock the n-GaAs Surface When Electrodepositing Bi From Acidic Solutions. *Electrochim. Acta* **2015**, *174*, 264–272. DOI: 10.1016/j.electacta.2015.05.188.

39. Sato, N. *Electrochemistry at Metal and Semiconductor Electrodes*; Elsevier Science B.V.: Amsterdam, The Netherlands, 1998. DOI: 10.1016/B978-0-444-82806-4.50015-5.

40. Oskam, G.; Long, J. G.; Natarajan, A.; Searson, P. Electrochemical Deposition of Metals on Silicon. *J. Phys. D: Appl. Phys.* **1998**, *31*, 1927-1949. DOI: 10.1088/0022-3727/31/16/001.

41. Erné, B. H.; Ozanam, F.; Chazalviel J. -N. The Mechanism of Hydrogen Gas Evolution on GaAs Cathodes Elucidated by In Situ Infrared Spectroscopy. *J. Phys. Chem. B* **1999**, *103*, 2948-2962. DOI: 10.1021/jp984765t.

42. Bard, A. J.; Faulkner, L. R. *Electrochemical Methods: Fundamentals and Applications;* John Wiley & Sons, Inc.: New York, USA, 1944.

43. Rajeshwar, K.; Mraz, T. The n-Gallium Arsenide Electrolyte Interface: Evidence for Specificity in Lattice Ion-Electrolyte Interactions, Dependence of Interfacial Potential Drops on Crystal Plane Orientation to the Electrolyte, and Implications for Solar Energy Conversion. *J. Phys. Chem.* **1983**, *87*, 742-744. DOI: 10.1021/j100228a010.

44. Scharifker, B.; Hills, G. Theoretical and Experimental Studies of Multiple Nucleation. *Electrochim. Acta* **1983**, *28*, 879-889. DOI: 10.1016/0013-4686(83)85163-9.

45. Rigano, P. M.; Mayer, C.; Chierchie, T. Electrochemical Nucleation and Growth of Copper on Polycrystalline Palladium. *J. Electroanal. Chem.* **1988**, *248*, 219-228. DOI: 10.1016/0022-0728(88)85163-5.

46. Cadle, S. H.; Bruckenstein, S. Ring-Disk Electrode Study of the Reduction of Bismuth on Platinum. *Anal. Chem.* **1972**, *44*, 1993-2001. DOI: 10.1021/ac60320a011.

47. Nosal-Wiercinska, A. The Kinetics and Mechanism of the Electroreduction of Bi(III) Ions From Chlorates (VII) With Varied Water Activity. *Electrochim. Acta* **2010**, *55*, 5917–5921. DOI: 10.1016/j.electacta.2010.05.045.

48. Mitsunaga, T. X-Ray Thin-Film Measurement Techniques. II. Out-of-Plane Diffraction Measurements. *The Rigaku J.* **2009**, *25*, 7-12.

49. Goodman, A. M.; Perkins, D. M. Metal Semiconductor Barrier Height Measurement by the Differential Capacitance Method—Degenerate One Carrier System. *J. Appl. Phys.* **1964**, *35*, 3351-3353. DOI: 10.1063/1.1713221.

50. Blakemore, J. S. Approximation for Fermi-Dirac Integrals, Especially the Function F_1/2(η) Used to Describe Electron Density in a Semiconductor. *Solid State Electron.* **1982**, *25*, 1067-1076. DOI: 10.1016/0038-1101(82)90143-5.

51. Reineke, R.; Memming, R. High Barrier GaAs/Metal Schottky Junctions Produced by Electrochemical Metal Deposition. *Surf. Sci.* **1987**, *192*, 66-80. DOI: 10.1016/S0039-6028(87)81162-7.

52. Schlesinger, R.; Rogaschewski, S.; Janietz, P. J. Electrochemically Deposited Copper Schottky Contacts on n-Type GaAs for Electron-Beam-Induced Current Measurements. *Phys. Status Solidi A* **1990**, *120*, 687-694. DOI: 10.1002/pssa.2211200243.

53. Rhoderick, E. H. Metal-semiconductor contacts. *IEE Proceedings I - Solid-State and Electron Devices* **1982**, *129*, 1-14. DOI: 10.1049/ip-i-1.1982.0001.

54. Padovani, F. A.; Stratton, R. Field and Thermionic-Field Emission in Schottky Barriers. *Solid-State Electron.* **1966**, *9*, 695-707. DOI: 10.1016/0038-1101(66)90097-9.

55. Rhoderick, E. H. The Physics of Schottky Barriers. *Rev. Phys.Tech.* **1970**, *1*, 1153-1167. DOI: 10.1088/0034-6683/1/2/302

56. Bimberg, D.; Blachnik, R.; Cardona, M.; Dean, P. J.; Grave, T.; Harbeke, G.; Hübner, K.; Kaufmann, U.; Kress, W.; Madelung, O.; et al. *Physics of Group IV Elements and III-V Compounds;* Springer-Verlag Berlin Heidelberg, Berlin, Germany, 1982.